Transition Met Chem
DOI 10.1007/s11243-016-0068-x

Syntheses, crystal structures, and DNA binding and catalytic properties of two transition metal coordination polymers constructed from 5-aminoisophthalic acid and bis-benzimidazole ligands

Yong-Hong Wen[1] · Xiao-Wei Mu[1] · Hui-Ling Wen[1]

Received: 22 March 2016 / Accepted: 27 May 2016

Abstract Two mixed-ligand transition metal coordination polymers, $\{[Co(aip)(bbp)]\cdot(H_2O)\}_n$ (**1**) and $\{[Ni_2(aip)(Hbbop)_2]\cdot(H_2O)_2\}_n$ (**2**) (H_2aip = 5-aminoisophthalic acid, bbp = 1,3-bis(benzoimidazol-2-yl)propane, H_2bbop = 1,3-bis(benzimidazol-2-yl)-2-oxapropane), were synthesized and characterized by elemental analyses, IR spectra, single-crystal X-ray diffraction, and thermogravimetric analyses. Complex **1** has a 1D chain structure, while **2** has a 3-connected 2D network with (6^3) topology. Both structures are further connected by hydrogen bonds and π–π stacking interactions to form the 3D supramolecular architectures. DNA binding and catalytic properties of the two complexes were investigated.

Introduction

There is increasing interest in the design and synthesis of transition metal coordination polymers, not only because of their potential applications as functional materials for luminescence, catalysis, and magnetism, but also because of their intriguing structures and topologies [1–4]. A number of coordination polymers with promising properties have been synthesized by the rational selection of metal centers and organic linkers [5–7]. In recent years, particular attention has been devoted to coordination polymers constructed from aromatic polycarboxylic acids and bis(nitrogen-containing heterocycles) as mixed organic building blocks [8–11]. These two types of organic ligand possess a variety of coordination modes suitable for the construction of polymeric structures. The degree of deprotonation or protonation of these compounds depends greatly on the pH of the reaction system, and they can act as both H-bond acceptors and donors to assemble supramolecular structures [12, 13]. Most of the transition metal coordination polymers reported to date use pyridyl- or imidazol-containing compounds as auxiliary ligands in metal–polycarboxylate systems [14–18]. To the best of our knowledge, studies on the mixed-ligand transition metal coordination polymers containing 5-aminoisophthalic acid (H_2aip) and bis-benzimidazole ligands have been scarcely reported [19]. To explore the use of mixed ligands to fabricate new architectures, we selected two structurally similar bis-benzimidazole compounds, 1,3-bis(benzoimidazol-2-yl)propane (bbp) and 1,3-bis(benzimidazol-2-yl)-2-oxapropane (H_2bbop) (Scheme 1), as auxiliary ligands and synthesized two transition metal coordination polymers, namely $\{[Co(aip)(bbp)]\cdot(H_2O)\}_n$ (**1**) and $\{[Ni_2(aip)(Hbbop)_2]\cdot(H_2O)_2\}_n$ (**2**). Both complexes have been characterized by elemental analyses, IR spectra, single-crystal X-ray diffraction, and thermogravimetric analyses. The DNA binding and catalytic properties of the complexes for the degradation of methyl orange by sodium persulfate in a Fenton-like process have been investigated.

Electronic supplementary material The online version of this article (doi:10.1007/s11243-016-0068-x) contains supplementary material, which is available to authorized users.

✉ Yong-Hong Wen
yonghwen@163.com

[1] State Key Laboratory Base of Eco-chemical Engineering, Laboratory of Inorganic Synthesis and Applied Chemistry, College of Chemistry and Molecular Engineering, Qingdao University of Science and Technology, Qingdao 266042, China

Published online: 18 June 2016

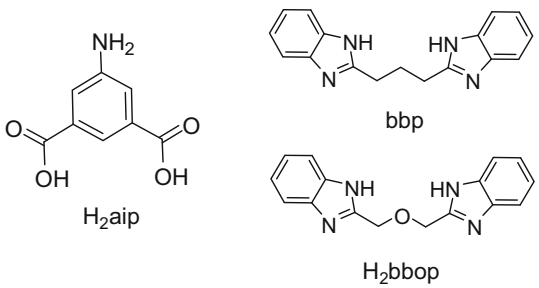

Scheme 1 Structural formulas of the ligands

Experimental

Materials and methods

All commercially available reagents and chemicals were of analytical-grade purity and used without further purification. The bis-benzimidazole compounds were prepared by literature procedures [20]. The C, H, and N contents were determined using an Elementar Vario EL III analyzer. Infrared spectra were recorded from KBr pellets on a Nicolet 510P FT-IR spectrometer. Thermogravimetric analyses (TGA) were performed on a Perkin-Elmer TG-7 analyzer heated from room temperature to 900 °C under air at heating rate of 10 °C min^{-1}.

Synthesis of complex 1

A mixture of $CoCl_2{\cdot}6H_2O$ (0.238 g, 1 mmol), 5-aminoisophthalic acid (0.181 g, 1 mmol), 1,3-bis(benzoimidazol-2-yl)propane (0.276 g, 1 mmol), 2 mL of 1 mol L^{-1} NaOH, and 8 mL of H_2O was placed in a Parr Teflon-lined stainless steel vessel (25 mL). The vessel was sealed and heated to 190 °C for 72 h and then cooled to room temperature, leading to the formation of block purple crystals of complex **1**. Yield 71 % (based on $CoCl_2{\cdot}6H_2O$). Anal. Calcd for $C_{25}H_{23}N_5O_5Co$ (%): C, 56.4; H, 4.4; N, 13.2. Found: 56.5; H, 4.4; N, 13.1. IR (KBr, cm^{-1}): 3630 (s), 3440 (m), 3179 (w), 3058 (w), 2937 (w), 1625 (w), 1603 (w), 1453 (s), 1414 (s), 1344 (m), 1293 (s), 1271 (m), 1220 (w), 1165 (w), 1150 (w), 1037 (w), 988 (w), 917 (w), 893 (w), 851 (w), 834 (w), 763 (w), 750 (s), 740 (s), 726 (m), 644 (w), 507 (m).

Synthesis of complex 2

A mixture of $NiCl_2{\cdot}6H_2O$ (0.475 g, 2 mmol), 5-aminoisophthalic acid (0.181 g, 1 mmol), 1,3-bis(benzimidazol-2-yl)-2-oxapropane (0.557 g, 2 mmol), 4 mL of 1 mol L^{-1} NaOH, and 6 mL of H_2O was placed in a Parr Teflon-lined stainless steel vessel (25 mL). The vessel was sealed and heated to 180 °C for 72 h. Upon cooling to room temperature, bronze-colored block crystals of **2** were obtained. Yield 67 % (based on $CoCl_2{\cdot}6H_2O$). Anal. Calcd for $C_{40}H_{35}N_9O_8Ni_2$ (%): C, 54.2; H, 4.0; N, 14.2. Found: C, 54.2; H, 3.9; N, 14.1. IR (KBr, cm^{-1}): 3640 (m), 3610 (m), 3400 (s), 1626 (m), 1609 (w), 1560 (s), 1530 (m),1490 (m), 1474 (m), 1458 (s), 1445 (m), 1421 (m), 1398 (s), 1320 (m), 1272 (m), 1236 (w), 1221 (m) 1112 (s), 1044 (w), 1003 (m), 785 (w), 759 (m) 737 (s), 710 (w) 631 (w), 550 (m), 528 (w), 496 (w), 436 (w).

Catalytic experiments

The catalytic behaviors of the complexes were investigated for the degradation of methyl orange using a standard process, as described in reference [21].

X-ray crystallography

Single-crystal X-ray diffraction data of two complexes were collected on a Bruker SMART 1000 CCD diffractometer with graphite-monochromated Mo$K\alpha$ radiation ($\lambda = 0.71073$ Å) using ω scan mode at room temperature. Intensity data were corrected for L_p factors, and an empirical absorption correction was applied. The structures of both complexes were solved by direct methods and expanded using Fourier differential techniques with SHELXTL [22]. All non-hydrogen atoms were located with successive difference Fourier syntheses. The structures were refined by full-matrix least squares methods on F^2 with anisotropic thermal parameters for all non-hydrogen atoms. The hydrogen atoms of water molecules in both complexes were located from the E-maps. The NH hydrogens involved in hydrogen bonding were also located from the difference Fourier maps and refined freely. The other hydrogen atoms were geometrically fixed and allowed to ride on their parent atoms. A summary of the key crystallographic data and structural refinements for the complexes is presented in Table 1. Selected bond distances and angles and the hydrogen bond data for both complexes are listed in Tables 2 and 3.

Results and discussion

Structure of $\{[Co(aip)(bbp)]\cdot(H_2O)\}_n$ (1)

Single-crystal X-ray diffraction analysis reveals that complex **1** crystallizes in the orthorhombic crystal system of space group $P2_12_12_1$. The asymmetric unit contains one Co(II) center, one anionic aip^{2-} ligand, one bbp ligand, and one crystal water molecule. The central Co(II) is five-coordinated by two nitrogen atoms from one bbp ligand, two oxygen atoms from one aip^{2-} ligand, and one oxygen atom from another aip^{2-} ligand (Fig. 1). The coordination

Table 1 Crystal data and structure refinement information of complexes **1** and **2**

Compounds	**1**	**2**
Formula	$C_{25}H_{23}N_5O_5Co$	$C_{40}H_{35}N_9O_8Ni_2$
Formula weight	532.41	887.15
Crystal system	Orthorhombic	Monoclinic
Space group	$P2_12_12_1$	C2/c
a(Å)	10.0078(2)	25.667(3)
b(Å)	14.0948(4)	9.4615(3)
c(Å)	17.8140(5)	20.467(2)
α(°)	90	90
β(°)	90	132.08(2)
γ(°)	90	90
V(Å^3)	2512.81(11)	3688.6(2)
Z	4	4
D (g cm^{-3})	1.407	1.597
μ (mm^{-1})	0.728	1.091
Crystal size (mm)	0.24 × 0.25 × 0.31	0.27 × 0.34 × 0.42
Total reflections	6587	6970
Unique reflections	4111	3261
R(int)	0.028	0.036
R_1^a (all data)	0.0426	0.0480
R_1^a [I > 2σ(I)]	0.0378	0.0397
wR_2^b (all data)	0.0844	0.1082
wR_2^b [I > 2σ(I)]	0.0807	0.1001
GOF on F^2	1.04	1.06
Max/min. residual (e Å^{-3})	0.29/−0.31	0.51/−0.49

[a] $R = \sum ||F_o| - |F_c|| \Big/ \sum |F_o|$

[b] $wR = \left[\sum w(F_o^2 - F_c^2) \Big/ \sum w(F_o^2)^2 \right]^{1/2}$

geometry of the cobalt is between trigonal bipyramidal and square pyramidal, with a t value of 0.49 [23]. The Co1–O3A gives a relatively long distance [2.390(2) Å] and the O3A–Co1–O4A shows a relatively small angle [58.44(9)°] due to the chelating coordination of the carboxylate group. The other coordinated bond lengths [Co–O 1.976(2) and 2.038(2), Co–N 2.023(3) and 2.034(3) Å] and angles [91.18(9) –120.14(11)°] fall in the normal ranges found in the structurally related complexes [24–26]. Each aip^{2-} ligand bridges two metal centers to form a 1D chain in the a direction, with Co–Co distances of 10.008 Å (Fig. 2a). Intermolecular N3–H3···O4 [2.827(4) Å] and N1–H1B···O3 [3.217(4) Å] hydrogen bonds connect the 1D chain into a 2D net structure (Fig. 2b). The 2D networks are further connected by intermolecular hydrogen bonds, O1W–H1WB···N1 [O1W···N1 2.988(7) Å], O1W–H1WB···O2 [O1W···O2 2.840(5) Å], and N4–H4···O1W [N4···O1W 2.737(5) Å] to form a 3D supramolecular structure (Fig. S1 in Supporting Information). In addition, there are C2–H2···O3 [C2···O3 2.766(4) Å], C16–H16B···O2 [C16···O2 3.215(4) Å], and C18–H18B···O3 [C18···O3 3.260(5) Å] hydrogen bonds.

Structure of $\{[Ni_2(aip)(Hbbop)_2]\cdot(H_2O)_2\}_n$ (2)

Substitution of the methylene group in bbp by an oxygen atom gives bbop. Complex **2** has a two-dimensional structure, and crystallizes in the monoclinic crystal system of space group $C2/c$. As shown in Fig. 3, complex **2** consists of two Ni(II) centers, one anionic aip^{2-} ligand, two anionic $Hbbop^-$ ligands, and two water molecules. The asymmetric unit of **2** contains half the molecule, which is related to the other half by a crystallographic twofold axis. The Ni(II) center is five-coordinated by two oxygen atoms, one from an aip^{2-} ligand and another from a $Hbbop^-$ ligand, plus three nitrogen atoms, two from one $Hbbop^-$ ligand and one from another $Hbbop^-$ ligand. The coordination geometry of the metal is between trigonal bipyramidal and square pyramidal, with a t value of 0.51 [23]. The axial positions are occupied by O1 and O3 with an

Table 2 Selected bond lengths (Å) and angles (°) for complexes **1** and **2**

Complex **1**			
Co1–O1	1.976(2)	Co1–O3A[a]	2.390(2)
Co1–N2	2.034(3)	Co1–O4A[a]	2.038(2)
Co1–N5	2.023(3)		
O1–Co1–N2	108.42(11)	N2–Co1–N5	110.57(11)
O1–Co1–N5	109.28(11)	O4A[a]–Co1–N2	114.89(11)
O1–Co1–O4A[a]	91.18(9)	O4A[a]–Co1–N5	120.14(11)
Complex **2**			
Ni1–O1	2.013(3)	Ni1–N4	2.021(2)
Ni1–O3	2.169(3)	Ni1–N5C[b]	2.036(3)
Ni1–N2	2.049(3)		
O1–Ni1–O3	170.30(12)	O3–Ni1–N4	76.76(10)
O1–Ni1–N2	97.85(12)	O3–Ni1–N5C[b]	96.20(12)
O1–Ni1–N4	104.20(11)	N2–Ni1–N4	140.05(9)
O1–Ni1–N5C[b]	92.70(12)	N2–Ni1–N5C[b]	104.17(11)
O3–Ni1–N2	76.26(11)	N4–Ni1–N5C[b]	107.55(12)

Symmetry codes: [a] $1 + x, y, z$; [b] $3/2 - x, -1/2 + y, 3/2 - z$

Table 3 Hydrogen bond data (Å) and (°) for complexes **1** and **2**

D–H…A	d(D–H)	d(H…A)	d(D…A)	∠DHA
Complex **1**				
O1W–H1WB···N1[a]	0.80(5)	2.45(5)	2.988(7)	126(6)
O1W–H1WB···O2[b]	0.80(5)	2.39(7)	2.840(5)	117(6)
N3–H3···O4[c]	0.84(3)	1.99(3)	2.827(4)	177
N1–H1B···O3	0.86(3)	2.69	3.217(4)	125
N4–H4···O1 W	0.84(3)	1.96(4)	2.737(5)	155(4)
C2–H2···O3	0.93	2.44	2.766(4)	100
C16–H16B···O2	0.97	2.43	3.215(4)	138
C18–H18B···O3[d]	0.97	2.43	3.260(5)	144
Complex **2**				
O1W–H1WA···O2	0.85(7)	2.01(7)	2.863(6)	177(9)
O1W–H1WB···N1[e]	0.85(9)	2.23(10)	3.074(8)	175(6)
N3–H3···O2[f]	0.80(5)	2.03(5)	2.698(4)	141
C13–H13B···O1W[g]	0.97	2.59	3.410(8)	146
C14–H14A···O1 [h]	0.97	2.45	3.029(5)	118

Symmetry codes: [a] $3/2 - x, 1 - y, ½ + z$; [b] $½ + x, 3/2 - y, 1 - z$; [c] $1 - x, -1/2 + y, ½ - z$; [d] $1 + x, y, z$; [e] $x, 1 + y, z$; [f] $3/2 - x, ½ - y, 2 - z$; [g] $½ + x, ½ - y, ½ + z$; [h] $3/2 - x, ½ + y, 3/2 - z$

O1–Ni1–O3 angle of 170.30(12)°, and the equatorial positions are occupied by N2, N4, and N5C with the sum of the angles N2–Ni1–N4, N2–Ni1–N5C, and N4–Ni1–N5C being 351.77°. All coordinated bond lengths (Ni–O 2.013(3)–2.169(3) Å, Ni–N 2.021(2)–2.049(3) Å) are comparable with those in related Ni(II) complexes [27, 28]. Atom N5 of the $Hbbop^-$ ligand is deprotonated. The

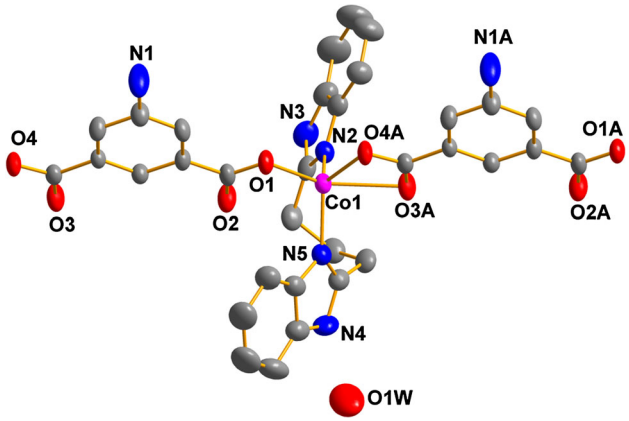

Fig. 1 The molecular structure and coordination environment of **1**. Hydrogen atoms are omitted for clarity. Symmetry codes: A = $1 + x$, y, z

deprotonated $Hbbop^-$ anion, acting as both chelating-tridentate and bridging-monodentate ligand, connects metal centers to form a 1D chain (Fig. 4). The two benzimidazole rings in $Hbbop^-$ are nearly coplanar such that the dihedral angle between them is 39.4(2)°. The 1D chains are further linked by aip^{2-} ligands to form a 2D layer (Fig. 5). In the 2D layer, the distances between Ni atoms connected by $Hbbop^-$ and aip^{2-} ligands are 5.928(2) and 10.266(2) Å, respectively. From a topological point of view, both $Hbbop^-$ and aip^{2-} ligands can be regarded as linkers between the Ni(II) centers. Therefore, the framework of **2** can be described as a 3-connected network with (6^3) topology (Fig. 5). Four types of hydrogen bonds are found in **2**: specifically O–H···O (O···O = 2.863(6) Å), N–H···O (N···O = 2.698(4) Å), O–H···N (O···N = 3.074(8) Å), and C–H···O (C···O = 3. 029(5), 3.410 (8) Å) contacts (Table 3). The 2D networks are connected by intermolecular hydrogen bonds and short aromatic ring π–π stacking interactions to form a 3D supramolecular structure (Fig. S2 in Supporting Information). The centroid–centroid distance between the imidazole rings of the neighboring layers is 3.528(2) Å.

Coordination modes of organic ligands in complexes 1 and 2

It can be seen from the structure descriptions above that the three organic ligands adopt different coordination modes. Although aip^{2-} anions bridge two mental centers in both complexes **1** and **2**, in complex **1**, one carboxylate group of aip^{2-} adopts a $\mu_1 - \eta^0{:}\eta^1$ mode, and the other adopts $\mu_1 - \eta^1{:}\eta^1$ coordination (mode I, Scheme S1 in Supporting Information). In complex **2**, both carboxylate groups of aip^{2-} adopt $\mu_1 - \eta^1{:}\eta^0$ coordination (mode II, Scheme SI).

The two structurally similar bis-benzimidazole ligands also reveal different coordination modes. The neutral bbp

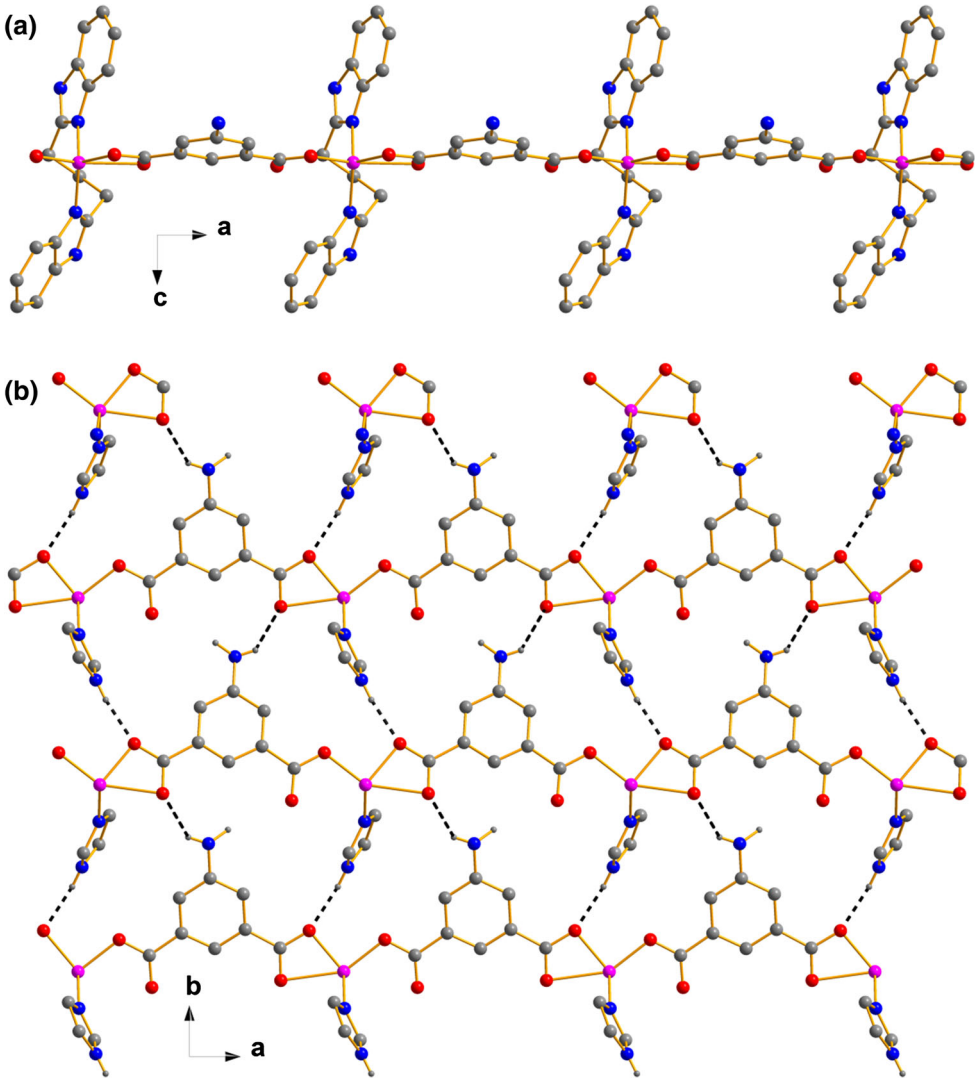

Fig. 2 **a** The 1D chain structure of **1** viewing along *b axis*. **b** The 2D net structure of **1** formed by hydrogen bonds (*dash lines*). The *imidazole rings* in bbp ligands are shown only for clarity

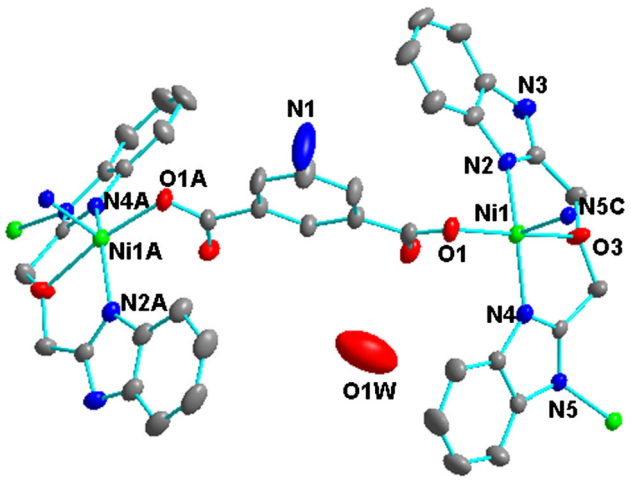

Fig. 3 The molecular structure and coordination environment of **2**. The hydrogen atoms are omitted for clarity. Symmetry codes: A = 1 − *x*, *y*, 3/2 − *z*; C = 3/2 − *x*, −1/2 + *y*, 3/2 − *z*

ligand in complex **1** shows chelating coordination modes (mode III, Scheme S1). In complex **2**, the deprotonated $Hbbop^-$ anion exhibits chelating-tridentate and bridging-monodentate coordination modes (mode IV, Scheme S1).

Thermal analysis

Thermogravimetric analyses were carried out for both complexes (Fig. S3 in Supporting Information). Complex **1** shows a 3.33 % weight loss from 140 to 335 °C, corresponding to the loss of one lattice water molecule (calcd 3.38 %). The second weight loss from 335 to 520 °C corresponds to decomposition of the organic components (obsd 81.90 %, calcd 82.53 %). The residual mass of 15.31 % corresponds to the formation of Co_2O_3 (calcd 14.07 %). Complex **2** shows a 4.22 % weight loss from 100 to 310 °C, corresponding to the loss of two water molecules (calcd 4.06 %). The second weight loss from 310 to

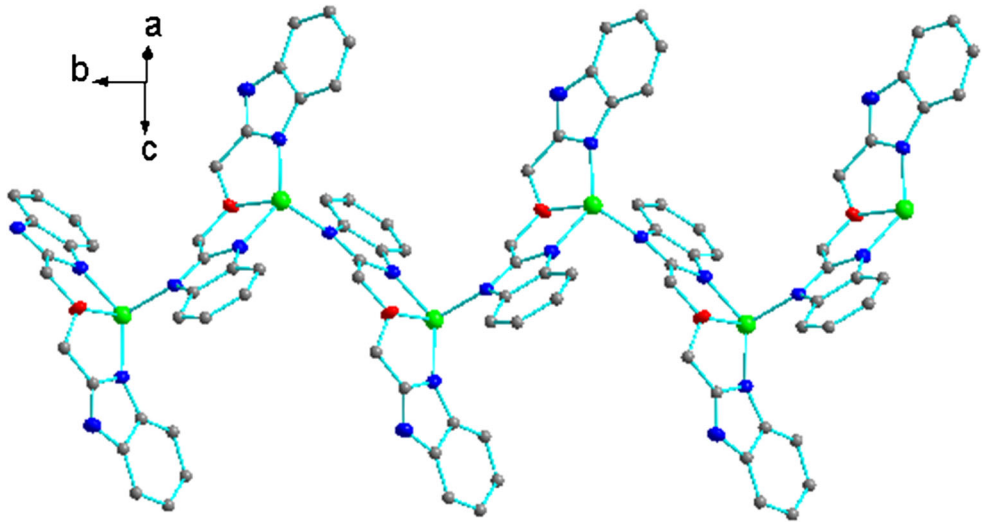

Fig. 4 The 1D chain structure of **2** along *b axis*

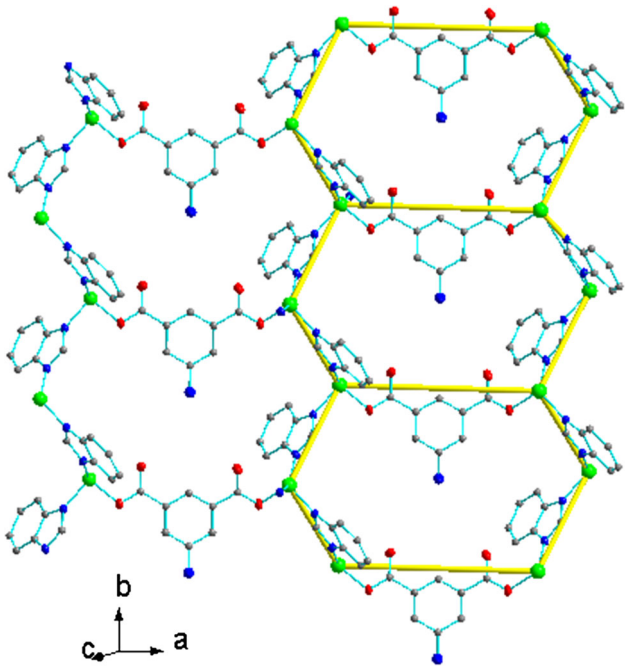

Fig. 5 The 2D layer and simplified (6^3) topology structure of **2**. The only bridging benzimidazoles in $Hbbop^-$ ligands are shown for clarity

550 °C can be assigned to decomposition of the organic components (obsd 76.81 %, calcd 79.09 %). The remaining residue of 15.97 % corresponds to the formation of NiO (calcd 16.86 %).

DNA binding studies

Electronic absorption spectroscopy is an effective method to examine the binding modes of metal complexes with DNA. Electronic absorption spectra of both complexes were recorded in the range of 200–600 nm (Figs. 6, 7). The lower wavelength peaks (255 nm for both **1** and **2**) can be assigned to intraligand $\pi \rightarrow \pi^*$ transitions of the benzene ring in the aip^{2-} ligand, while the higher wavelength peaks can be assigned to intraligand $\pi \rightarrow \pi^*$ transitions of benzimidazole in the bbp or Hbbop ligands, respectively. In Fig. 6, only a single peak is observed at 271 nm, while in Fig. 7, two absorption peaks are seen at 271 and 275 nm. This indicates that both benzimidazole rings are in the same chemical environment in complex **1**, whereas the two benzimidazole rings are in different chemical environments in complex **2**, in agreement with the single-crystal structure analysis.

It can be seen from Figs. 6 and 7 that the absorption spectra of both **1** and **2** show decreases after adding ssDNA or dsDNA to the solutions of the complexes, but none of the absorptions show red shifts **2**. This suggests that the interaction between these complexes and DNA might be electrostatic in nature [29].

DNA binding properties of complexes **1** and **2** were studied by UV–vis titration experiments. In these experiments, 20-μL solutions of DNA (6.551×10^{-5} mol L^{-1} for **1**, and 4.397×10^{-5} mol L^{-1} for **2**) were each added to 3.0 mL of a solution of the complex (2.831×10^{-4} mol L^{-1} for **1**, and 1.702×10^{-4} mol L^{-1} mol L^{-1} for **2**) by a micropipette. Because of the limited solubility of these complexes in water, the titration experiments were carried out in the presence of a small amount of DMSO. The intrinsic binding constants K_b were determined from the resulting absorbance data at the specified wavelength using the following equation [30]:

$$[\mathrm{DNA}]/(\varepsilon_a - \varepsilon_f) = [\mathrm{DNA}]/(\varepsilon_b - \varepsilon_f) + 1/K_b(\varepsilon_b - \varepsilon_f)$$

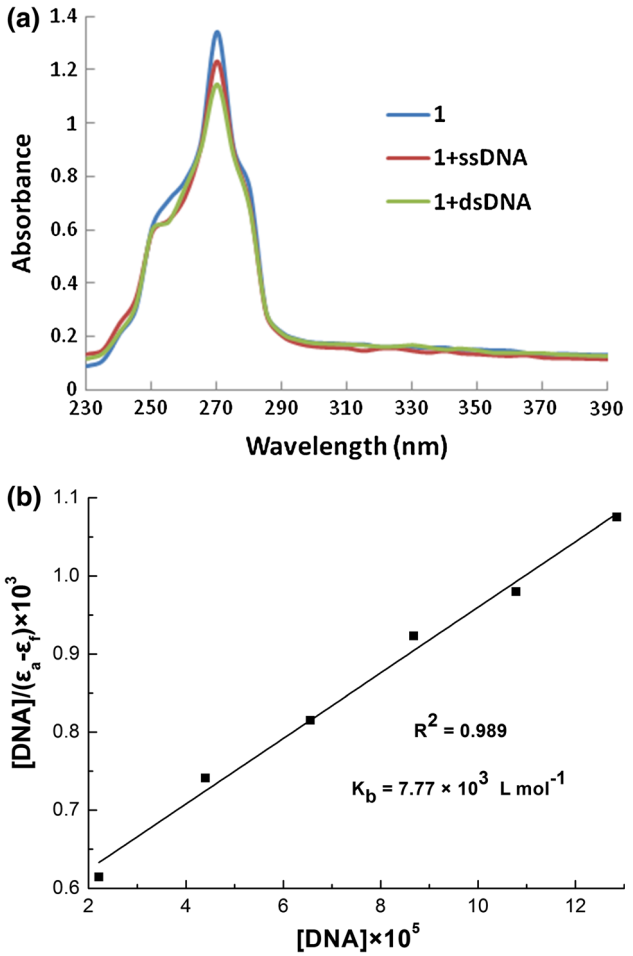

Fig. 6 **a** UV–vis absorption spectra of complex **1** (2.831×10^{-4} mol L^{-1}) and **1** + DNA (6.551×10^{-5} mol L^{-1}). **b** Plot of [DNA]/($\varepsilon_a - \varepsilon_f$) versus [DNA] for absorption titration of dsDNA with complex **1**

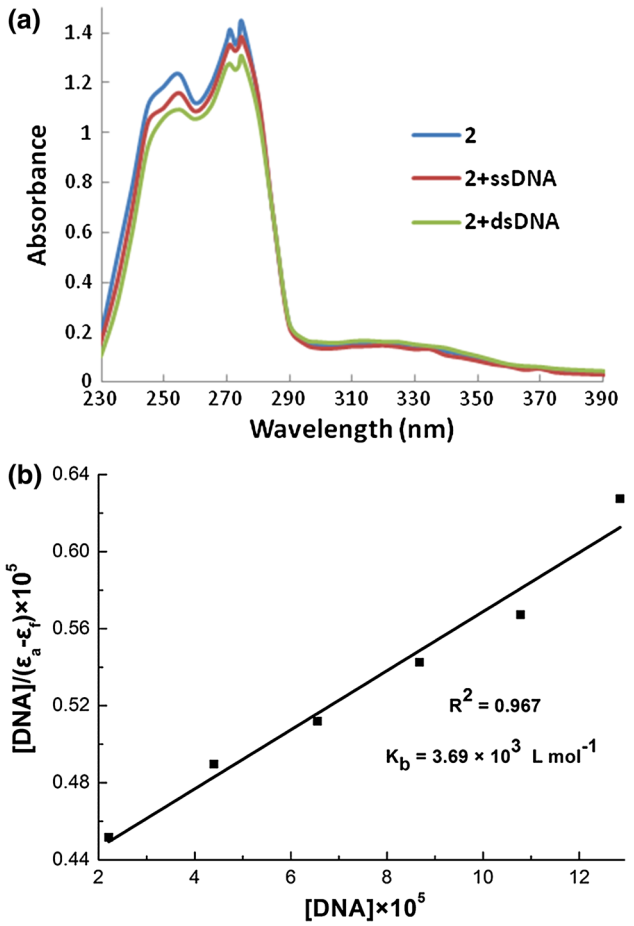

Fig. 7 **a** UV–vis absorption spectra of complex **2** (1.702×10^{-4} mol L^{-1}) and **2** + DNA (4.397×10^{-5} mol L^{-1}). **b** Plot of [DNA]/($\varepsilon_a - \varepsilon_f$) versus [DNA] for absorption titration of dsDNA with complex **2**

where [DNA] is the concentration of DNA and ε_f, ε_a, and ε_b refer to the extinction coefficients for the free complex, after each addition of DNA to the complex, and for the complex in the fully bound form, respectively. Plots of [DNA]/($\varepsilon_a - \varepsilon_f$) versus [DNA] gave straight lines. The binding constants K_b obtained from the ratio of slope to intercept were 7.77×10^3 L mol^{-1} for **1** (Fig. 6) and 3.69×10^3 L mol^{-1} for **2** (Fig. 7). These K_b values are comparable to those of bis-benzimidazole Cd(II) complexes {2.3×10^4 L mol^{-1} for $[Cd(bbtp)_2]\cdot(pic)_2$ (bbtp = 1,3-bis((1-ethylbenzimidazol-2-yl)-2-thiapropane)) [31], 2.19×10^4 L mol^{-1} for $[Cd(bbmt)_2(CH_3OH)_2]\cdot(NO_3)_2$ (bbmt = 2,5-bis((benzoimidazol-2-yl)methylthio)-1,3,4-thiadiazole)) [32], and 9.06×10^4 L mol^{-1} for $[Cd(bbp)_2](pic)_2\cdot 2DMF$ (bbp = 2,6-bis(2-benzimidazolyl)pyridine) [33]}, and also similar to those of bis-benzimidazole Co(II) complexes {1.48×10^4 L mol^{-1} for $[Co(HL)(bbop)]_n$ (H_3L = 5-(carboxymethoxy)isophthalic acid) and 4.03×10^4 L mol^{-1} for $[Co(HL)(bbe)]_n$ (bbe = 1,2-bis(benzoimidazol-2-yl)ethane)} [26], but smaller than those of non-benzimidazole Cd(II) complexes {7.62×10^5 L mol^{-1} for $[Cd(5\text{-Br-salo})_2(CH_3OH)]_2$ (5-Br-salo = 5-bromo-salicylaldehyde), 1.36×10^5 L mol^{-1} for $[Cd(5\text{-Br-salo})_2(phen)]_2$ (phen = 1,10-phenanthroline), and 3.83×10^6 L mol^{-1} for $[Cd(5\text{-Br-salo})_2(dpamH)]_5$ (dpamH = 2,2′-dipyridylamine)} [34]. The choice of organic ligands, metal ions, and the resulting structures of the complexes may all affect the resulting binding affinities with DNA.

Catalytic degradation of methyl orange

Transition metal coordination polymers constructed from aromatic polycarboxylic acids and bis(nitrogen-containing heterocycles) have the potential to act as catalysts for the degradation of organic pollutants such as azo dyes [27, 28]. Therefore, the catalytic activities of these complexes for the degradation of methyl orange by sodium persulfate are

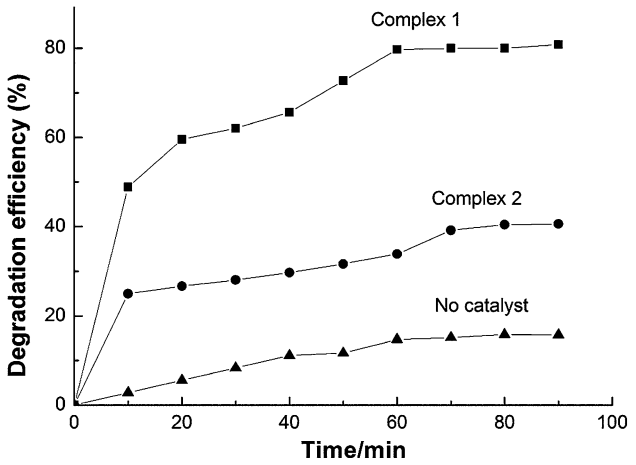

Fig. 8 The catalytic degradation of methyl orange with complexes **1** and **2**

investigated. The results (Fig. 8) showed that the degradation of methyl orange reaches 80 % after 60 min in the presence of complex **1**. For complex **2**, the degradation rate is slower, reaching 33.8 % under the same conditions, and only 40.6 % after 95 min. Hence, the Co(II) complex is a better catalyst than the Ni(II) complex for the degradation of methyl orange by sodium persulfate in a Fenton-like process. Similar results have been reported previously [27, 28]; the efficiencies of degradation of methyl orange under the same conditions by $[Co(mbix)(mip)]_n$, $[Ni(mbix)(ip)]_n$, and [Ni(mbix)(mip)] (mbix = 1,3-bis(imidazol-l-yl-methyl)benzene, H_2ip = isophthalic acid, H_2mip = 5-methylisophthalic acid) are 86, 65, and 38 %, respectively [27], while the efficiencies of degradation of methyl orange by $[Co(4,4'\text{-bpy})_2(H_2bptc)]$ and $[Ni(4,4'\text{-bpy})](H_2bptc)$ (4,4′-bpy = 4,4′-bipyridine, H_4bptc = 3,3′,4,4′-biphenyltetracarboxylic acid) are 95.6 and 48.3 %, respectively [28].

Conclusion

Two mixed-ligand transition metal coordination polymers were obtained by the hydrothermal reactions of two structurally related bis-benzimidazole ligands with 5-aminoisophthalic acid. The two coordination polymers are connected by hydrogen bonds and π–π stacking interactions to form 3D supramolecular architectures. The degree of deprotonation and coordination modes of the N-containing ligands and supramolecular interactions play a key role in the construction of these complexes. The complexes showed similar DNA binding abilities. The Co(II) complex displays higher catalytic activity than the Ni(II) complex for the Fenton-like degradation of methyl orange at room temperature.

Supplementary material

Crystallographic data for the structural analysis of the compounds have been deposited with the Cambridge Crystallographic Data Centre. CCDC reference numbers 1449760 for **1** and 1449763 for **2** contain the supplementary crystallographic data for this paper. These data can be obtained free of charge from the Cambridge Crystallographic Data Centre via www.ccdc.cam.ac.uk/data_request/cif.

Acknowledgments This work was supported by the National Natural Science Foundation of China (No. 20971076).

References

1. Farha OK, Malliakas CD, Kanatzidis MG, Hupp JT (2009) J Am Chem Soc 132:950–952
2. Allendorf MD, Bauer CA, Bhaktaa RK, Houka RJT (2009) Chem Soc Rev 38:1330–1352
3. Gong Y, Zhang MM, Hua W, Sun JL, Shi HF, Jiang PG, Liao FH, Lin JH (2014) Dalton Trans 43:145–151
4. Meng F, Fang Z, Li Z, Xu W, Wang M, Liu Y, Zhang J, Wang W, Zhao D, Guo X (2013) J Mater Chem A 1:7235–7241
5. Gu ZG, Xu XX, Zhou W, Pang CY, Bao FF, Li ZJ (2009) Chem Commun 48:3212–3214
6. Wen YH, Wang DM, Wen HL, Zhang Y, Yao K (2015) Z Anorg Allg Chem 641:1892–1898
7. Guo XG, Yang WB, Wu XY, Zhang QK, Lin L, Yu R, Chen HF, Lu CZ (2013) Dalton Trans 42:15106–15112
8. Hu JS, Shang YJ, Yao XQ, Qin L, Li YZ, Guo ZJ, Zheng HG, Xue ZL (2010) Cryst Growth Des 6:2676–2684
9. Kan WQ, Liu YY, Yang J, Liu YY, Ma JF (2011) CrystEngComm 13:4256–4269
10. Chen J, Feng YL, Jiang ZG, Cheng JW (2011) CrystEngComm 13:6071–6076
11. Wang GY, Yang LL, Li Y, Song H, Ruan WJ, Chang Z, Bu XH (2013) Dalton Trans 42:12865–12868
12. Abourahma A, Moulton B, Kravtsov V, Zaworotko MJ (2002) J Am Chem Soc 124:9990–9991
13. Liu YY, Ma JF, Yang J, Su ZM (2007) Inorg Chem 46:3027–3037
14. Lucas JS, Bell LD, Gandolfo CM, LaDuca RL (2011) Inorg Chim Acta 378:269–279
15. Karmakar A, Titi HM, Goldberg I (2011) Cryst Growth Des 11:2621–2636
16. Liu JQ, Wang YY, Huang YS (2011) CrystEngComm 13:3733–3740
17. Karmakar A, Goldberg I (2011) CrystEngComm 13:350–366
18. Wang GH, Lei YQ, Wang N, He RL, Jia HQ, Hu NH, Xu JW (2010) Cryst Growth Des 10:534–540
19. Yang Y, Yan LT, Luo XJ, Qin RH, Duan WG (2012) Supramol Chem 24:810–818
20. Liu HY, Wu H, Yang J, Liu YY, Liu B, Liu YY, Ma JF (2011) Cryst Growth Des 11:2920–2927
21. Chen MS, Deng YF, Zhang CH, Xu JH, Yi ZJ, Liang FP (2014) Transit Met Chem 39:901–907
22. Sheldrick GM (2008) Acta Crystallogr A 64:112–122
23. Addison AW, Nageswara RT, Reedijk J, Rijn VJ, Verschoor GC (1984) J Chem Soc, Dalton Trans 13:1349–1356

24. Wen YH, Xu GF, Yao K, Dou RT, Guo JX (2014) Z Anorg Allg Chem 640:2091–2096
25. Wen YH, Dou RT, Yao K, Xu GF (2015) J Coord Chem 68:38–54
26. Wen HL, Wang DM, Mu XW, Wen YH (2015) Transit Met Chem 40:509–517
27. Hao JM, Zhao YN, Yu BY, Hecke KV, Cui GH (2014) Transit Met Chem 39:741–753
28. Zhang YQ, Wang CC, Guo XX, Wang P (2016) Transit Met Chem 41:15–24
29. Long EC, Barton JK (1990) Acc Chem Res 23:271–273
30. Baguley BC, Bret ML (1984) Biochemistry 23:937–943
31. Wu HL, Wang KT, Kou F, Jia F, Liu B, Yuan JK, Bai Y (2011) J Coord Chem 64:2676–2687
32. Wen YH, Chen YY, Wen HL, Xie XL, Wang L (2012) J Coord Chem 65:2780–2792
33. Wu HL, Yuan JK, Huang XC, Kou F, Liu B, Jia F, Wang KT, Bai Y (2012) Inorg Chim Acta 390:12–21
34. Zianna A, Ristovic MS, Psomas G, Hatzidimitriou A, Coutouli-Argyropoulou E, Lalia-Kantouri M (2016) Polyhedron 107:136–147